ARTICLES

Measurements of OH^- absorption and proton activation in $Pb_{1-x}Ba_xNb_2O_6$ crystals with applications to holographic storage

Myeongkyu Lee and Robert S. Feigelson
Department of Materials Science & Engineering, Stanford University, Stanford, California 94305

Alice Liu and Lambertus Hesselink
Department of Electrical Engineering, Stanford University, Stanford, California 94305

Roger K. Route
Ginzton Laboratory, Stanford University, Stanford, California 94305

(Received 17 April 1997)

$Pb_{1-x}Ba_xNb_2O_6$ is a material under consideration for electro-optic and photorefractive applications. Single crystals of $Pb_{1-x}Ba_xNb_2O_6$ have been grown using the vertical Bridgman method in the composition range $0.5<1-x<0.6$. The formation and thermal fixing of holographic gratings in these crystals were recently demonstrated. In this study the OH^- absorption spectra were measured by fourier-transform infrared spectrometry. As-grown crystals showed a strong OH^- absorption near $\nu=3485\ cm^{-1}$, revealing the existence of protons (H^+) which are essential for the thermal fixing of holograms. The dependence of the integrated OH^- optical-absorption intensity on polarization showed that all of the O-H bonds were polarized either perpendicular or parallel to the *c* axis, with a greater proportion perpendicular. The proton concentration could be increased by heat treatment in a humid atmosphere and decreased in an ambient or oxygen atmosphere. The diffusivity of protons perpendicular to the *c* axis was measured in $Pb_{0.5}Ba_{0.5}Nb_2O_6$ by proton in-diffusion experiments and was found to be $D_0\approx0.219\times10^{-6}\ cm^2/s$ at 750 °C, which is comparable to the proton diffusivity in TiO_2 ($D_0\approx0.190\times10^{-6}\ cm^2/s$) and $LiNbO_3$ ($D_0=0.193\sim2.507\times10^{-6}\ cm^2/s$) at the same temperature. Measurements of the thermal decay of holograms showed that the proton activation energy, ΔE, in $Pb_{0.5}Ba_{0.5}Nb_2O_6$ was 0.95 ± 0.05 eV, which is close to the proton activation energies reported for $LiNbO_3$ and $KNbO_3$, 1.10–1.40 eV and 0.81–1.04 eV, respectively. [S0163-1829(97)02437-5]

I. INTRODUCTION

For certain electro-optic and photorefractive applications, such as holographic data storage, the concentration and activation of protons (H^+) can be very important. Amodei and co-workers,[1,2] demonstrated in 1971 that they could thermally fix holograms in $LiNbO_3$. They found that at elevated temperatures of around 150 °C, mobile ions compensated the electronic space charge fields built up during the writing process at room temperature. By erasing the electronic space charge fields with intense illumination, the remaining pure ionic space charge fields remained stable against erasure during readout at room temperature. These ions were known to be positively charged and were later identified as protons (H^+) by spatially resolved IR absorption measurements.[3] Protons are often present in as-grown oxide crystals in the form of hydroxyl ions (OH^-). The existence of protons can easily be revealed by infrared absorption spectroscopy from which protons can be characterized via the stretching mode of the O-H dipole whose vibrational frequency is around $3500\ cm^{-1}$. Such IR absorption studies have been reported for $SrTiO_3$,[4,5] $BaTiO_3$,[6,7] TiO_2,[8] $LiNbO_3$,[9–11] and $Sr_{0.61}Ba_{0.39}Nb_2O_6$.[12]

$Pb_{1-x}Ba_xNb_2O_6$ (PBN), a tungsten bronze ferroelectric, has recently emerged as a very promising material for electro-optic and photorefractive applications because of its very high electro-optic coefficients, particularly near the morphotropic phase boundary ($1-x=\sim0.63$).[13] PBN was discovered around 1960,[14,15] but since then not much work has been done on this material, in particular, with respect to photorefractive applications, mainly because of the difficulty in preparing large, optical-quality single crystals of controlled compositions. Although single crystals a few millimeters in size have been grown by the Czochralski method, the rapid loss of PbO from the melt has led to poor control over stoichiometry and compositional homogeneity.[16,17] Our approach utilizes the vertical Bridgman method with a sealed Pt crucible containing the charge material. Unidirectional solidification under a strong axial temperature gradient produced transparent single crystals without the loss of PbO. Crystal dimensions were limited, however, due to the fact that PBN crystals do not appear to grow readily in the radial direction. ''Bootstrapping'' to full-diameter seeds of centimeter dimensions is therefore difficult. Large PBN single crystals ($\sim2\ cm\times1\ cm\times1\ cm$) have been successfully grown using $Sr_{0.61}Ba_{0.39}Nb_2O_6$ (SBN61) single-crystal seeds. $Sr_{1-x}Ba_xNb_2O_6$ (SBN) has the same tungsten bronze structure and is commercially available. Crystal growth issues will be reported separately.

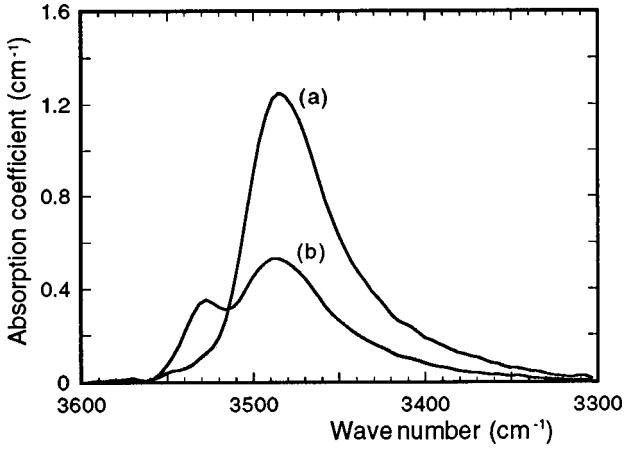

FIG. 1. The OH^- absorption spectra obtained with unpolarized light (a) propagating along the c axis and (b) propagating in the a-b plane.

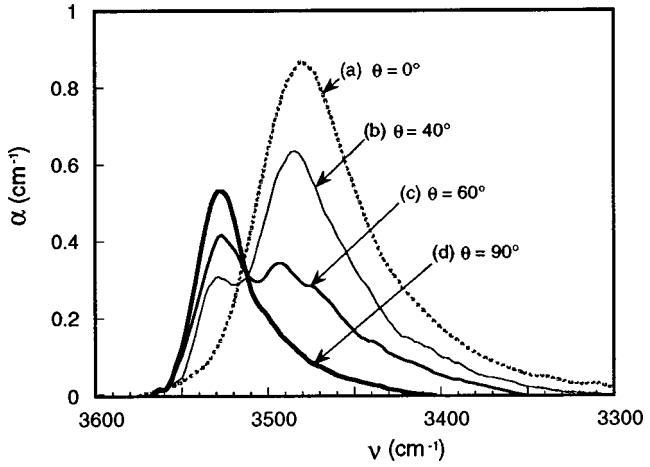

FIG. 2. Absorption spectrum versus polarization angle θ. θ was defined as the angle between the electric field vector of linearly polarized light and the a-b plane.

Another encouraging feature of PBN is that unlike SBN, as-grown crystals contained a high concentration of protons.[18] In addition, the concentration of protons can be increased or decreased by appropriate heat treatment. We have recently demonstrated the formation and thermal fixing of holographic gratings in this material.[19] It was also found that the fixing efficiency, defined as the ratio of the diffraction efficiency of a fixed grating to that of an unfixed grating, increased with increasing proton concentration.[20] An efficiency of about 80% could be achieved under optimum fixing conditions. The activation and diffusion of protons are therefore crucial for the thermal fixing of holograms. Through the use of the OH^- absorption measurements, the polarization and concentration of the O-H bonds in PBN crystals have been determined, along with the proton (H^+) diffusion behavior. A study of proton (H^+) activation is also presented together with the thermal decay of holograms.

II. SAMPLE PREPARATION AND ABSORPTION MEASUREMENTS

Single crystals of $Pb_{1-x}Ba_xNb_2O_6$ were grown by the vertical Bridgman method with compositions ranging from $1-x=0.50$ to 0.60. As-grown crystals containing the tetragonal phase showed a strong OH^- absorption, regardless of composition, although the absorption intensity varied from boule to boule. Selected $Pb_{0.5}Ba_{0.5}Nb_2O_6$ (PBN50) crystals chosen for detailed OH^- absorption measurements were fabricated in rectangular bars with faces perpendicular and parallel to the c axis.

The OH^- absorption spectra were obtained using fourier-transform infrared spectrometry in the wave number (ν) range from 3800 to 3200 cm^{-1} with a spectral resolution of 2–4 cm^{-1}. The baseline of the absorption spectrum was estimated by extrapolating the straight line segments to the left and right of the absorption band. The baseline was then subtracted from the spectrum to determine the absorption due to the OH^- stretching vibrations. A commercial four-plate ZnSe Brewster polarizer was used for the polarization measurements (This polarizer was designed for peak performance at 8–10 μm, but it works reasonably well over the range of 1–10 μm). For the high-temperature absorption measurements, a miniature oven was installed in the sample chamber of the spectrometer.

III. OH^- ABSORPTION SPECTRA IN $Pb_{0.5}Ba_{0.5}Nb_2O_6$

First, the absorption spectrum was measured with a small $Pb_{0.5}Ba_{0.5}Nb_2O_6$ crystal (1.9 mm×2.5 mm×2.3 mm) at room temperature. Unpolarized light propagating along the c axis with the electric fields in the a-b plane was utilized. As shown in Fig. 1(a), the spectrum obtained showed a maximum absorption near $\nu=3485$ cm^{-1} with a broadband shoulder on the low-energy side. A single Lorentzian or Gaussian curve could not be fitted to this spectrum, indicating the existence of at least two different energy states for the O-H bond in the a-b plane. The best fit was achieved with four or five individual bands including a very strong band centered at $\nu=3485$ cm^{-1} and several weak ones located in the low-energy shoulder region. The occurrence of multiple absorption bands is possible since there are several different hydrogen environments in the a-b plane of an unfilled tungsten bronze structure. The existence of one strong band indicates that protons prefer one specific site in the a-b plane. When the polarization of the incident light was rotated in the a-b plane, the intensity and shape of the absorption spectrum showed little change. If H^+ occupies a specific site in the a-b plane, four O-H bonds of the same kind will appear in the a-b plane within the unit cell, rotated by 90° with respect to each other because of the fourfold symmetry (4 mm) around the c axis. This will make the absorption intensity independent of the polarization direction in the a-b plane. From the IR absorption measurements alone, however, one cannot determine the absolute positions of the protons.

According to the work by Johnson, De Ford, and Shaner,[8] the OH^- ion concentration c_{OH} is given by

$$c_{OH}=\frac{\int \alpha\, d\nu}{a_{OH}\ln 10}, \tag{1}$$

where $\int \alpha\, d\nu$ is the integrated absorption intensity and a_{OH} is the absorption strength per ion. In order to determine the OH^- concentration, the value of a_{OH} must be known. Using the a_{OH} value for $LiNbO_3$ ($a_{OH}\approx 9.125\times10^{-18}$ cm) derived

by Klauer, Wöhlecke, and Kapphan,[21] the concentration of OH^- ions polarized in the a-b plane in this particular $Pb_{0.5}Ba_{0.5}Nb_2O_6$ crystal was estimated to be $\sim 4\times 10^{18}$ cm^{-3}.

When unpolarized light was propagated in the a-b plane, i.e., the electric fields had components both in the a-b plane and along the c axis, a new absorption band occurred with a peak absorption at the higher wave number of 3530 cm^{-1}, as illustrated in Fig. 1(b). It is believed that this is due to the O-H bonds vibrating along the c axis. In order to verify that the O-H bonds have polarizations both perpendicular to and along the c axis, the variation in absorption spectrum with incident light polarization was studied. Linearly polarized light was propagated along the b axis in the a-b plane and the polarization vector was inclined at an angle θ with respect to the a-b plane. Figure 2 shows the absorption spectra for several polarization angles θ. For $\theta=0°$, the absorption spectrum contained a fine structure with a peak absorption near 3485 cm^{-1}, as shown in Fig. 2(a). It should be noted here that the integrated absorption intensity was reduced in comparison to the case shown in Fig. 1(a) because the effective number of O-H bonds contributing to the absorption was decreased. (The O-H bonds polarized along the b axis did not contribute to the absorption in this case.) When θ was increased, the electric field developed a component in the direction of the c axis and a new absorption band appeared with a peak absorption at 3530 cm^{-1}. As θ was increased further, the absorption at 3530 cm^{-1} increased and the OH^- absorption band originally found in the a-b plane decreased. This indicates that the absorption band at 3530 cm^{-1} is due to O-H bonds directed along the c axis. Figure 2(d) shows the absorption spectrum along the c axis ($\theta=90°$). This band could not be fitted with a single Lorentzian or Gaussian peak either. That is, there apparently also exists more than one energy state for the O-H bond directed along the c axis. If all of the O-H bonds lie either in the a-b plane or along the c axis, the integrated absorption intensity, $I=\int \alpha\, d\nu$, at the polarization angle θ can be given by the following expression because the integrated absorption intensity is proportional to the number of absorbers:

$$I(\theta)=I(0°)\cos^2\theta+I(90°)\sin^2\theta, \tag{2}$$

where $I(0°)$ and $I(90°)$ are the integrated absorption intensities at $\theta=0°$ and $\theta=90°$, respectively. In Fig. 3, the measured integrated absorption intensity is plotted as a function of the polarization angle θ. The good agreement between the measured integrated intensity and the one expected from Eq. (2) confirms that all of the O-H bonds exist either in the a-b plane or along the c axis, with more O-H bonds polarized perpendicular to than along the c axis, assuming that the absorption strength a_{OH} is independent of the polarization of the O-H bond.

Figure 4 shows the absorption spectrum from the O-H bonds polarized in the a-b plane as a function of temperature, in which unpolarized light was propagated along the c axis. As already observed in Fig. 1(a), the spectrum obtained at room temperature shows a peak absorption near $\nu=3485$ cm^{-1}. This strong absorption at $\nu=3485$ cm^{-1} began to decrease with increasing temperature. The position of the peak absorption moved toward lower energies with a corresponding decrease in maximum intensity as the temperature increased. The absorption spectrum became broader and more symmetric with increasing temperature. All of these observations indicate that protons, which prefer a specific site at room temperature, tend to occupy an increasing number of different sites as the temperature increases.

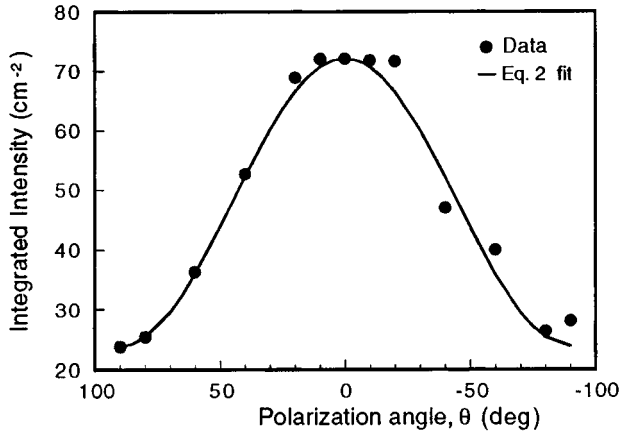

FIG. 3. Integrated absorption intensity as a function of polarization angle θ.

IV. HEAT TREATMENT AND PROTON DIFFUSION

The proton concentration could be changed by a high-temperature heat treatment, regardless of crystal composition. It increased with heat treatment in a humid atmosphere created by flowing water vapor into the hot furnace and decreased with heat treatment in an ambient or oxygen atmosphere. Figure 5 shows that the OH^- absorption, measured in PBN50 with the unpolarized light propagating perpendicular to the c axis, greatly increased after heat treatment in the humid atmosphere. It shows that the concentrations of O-H bonds both perpendicular to and along the c axis increased by almost the same proportion. The proton concentration reached saturation after a specific heat-treatment time, which depended on the sample dimension and the heat-treatment temperature. In an attempt to determine the proton diffusivity, a larger rectangular sample of dimensions 3.6 mm×3.1 mm×5.8 mm was isothermally heat treated at 750 °C in a humid atmosphere for a certain time t and then

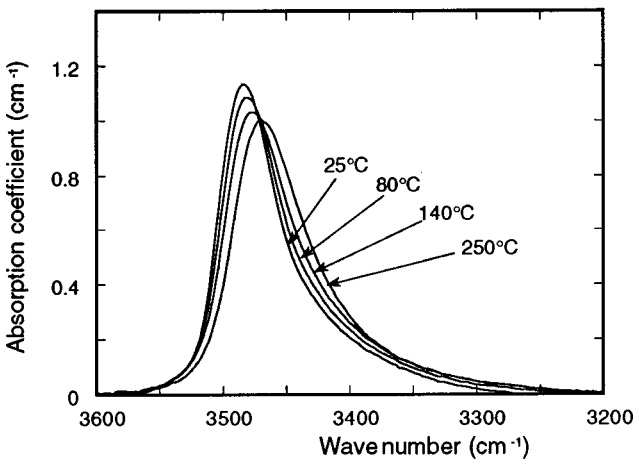

FIG. 4. OH^- absorption spectrum as a function of temperature.

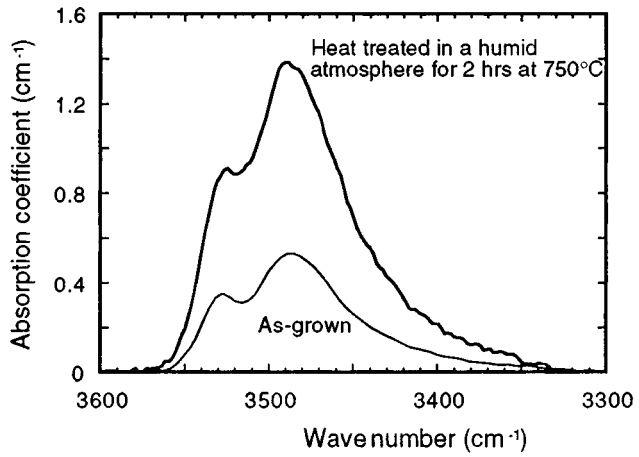

FIG. 5. Effect of the heat treatment on the OH^- absorption strength.

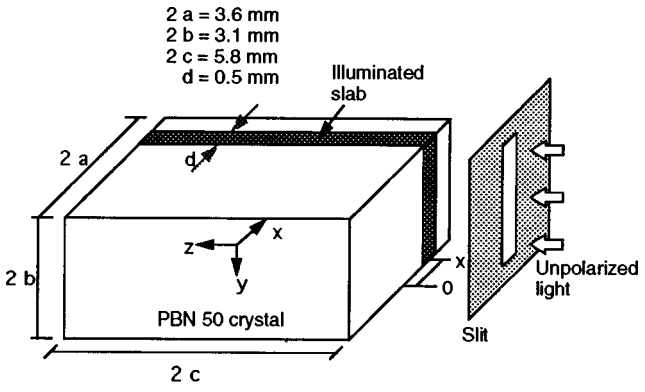

FIG. 6. Geometry for the position-dependent absorption measurements.

the position-dependent absorptions were measured at room temperature with a narrow slit scanned along the a axis, as shown in Fig. 6. This process, i.e., heat treatment at 750 °C and absorption measurement at room temperature, was repeated in order to obtain the proton concentration profile as a function of heat-treatment time. In the absorption measurements, the crystal was put as close to the slit as possible in order to reduce the effects of diffraction. The integrated absorption intensity from the illuminated slab (shaded in Fig. 6) will be proportional to the average proton concentration of the shaded slab according to Eq. (1). The concentrations of protons (H^+) whose O-H bonds are in the a-b plane were calculated from the measured integrated absorption intensities using the a_{OH} value for $LiNbO_3$. Figure 7 represents the average proton concentration of the slab, $\overline{C}(x,t)$, as a function of slab position x for different heat treatment times t, which shows a typical diffusion profile. The diffusion of protons in this case can be expressed by the following three-dimensional diffusion equation with the reference point at the center of the crystal:

$$\frac{\partial C(x,y,z,t)}{\partial t}=D_0\frac{\partial^2 C}{\partial x^2}+D_0\frac{\partial^2 C}{\partial y^2}+D_e\frac{\partial^2 C}{\partial z^2}, \tag{3}$$

where D_0 is the diffusivity along the a or b axis and D_e is the diffusivity along the c axis. The initial condition is

$$C(x,y,z,0)=C_0, \tag{4}$$

where C_0 is the initial concentration. Boundary conditions can be chosen as follows because of the large amount of water vapor flowing through the furnace:

$$\begin{aligned} &C(-a,y,z,t)=C(a,y,z,t)=C_s,\\ &C(x,-b,z,t)=C(x,b,z,t)=C_s, \quad (t>0)\\ &C(x,y,-c,t)=C(x,y,c,t)=C_s, \end{aligned} \tag{5}$$

where C_s is the saturation concentration which can be experimentally determined (a, b, and c are defined in Fig. 6). This type of equation with the above initial and boundary conditions is frequently encountered in heat conduction and mass transport and can be easily solved by the separation of variables. The solution to Eq. (3) is given by[22]

$$\begin{aligned} C(x,y,z,t)=C_s-&\frac{64(C_s-C_0)}{\pi^3}\\ &\times\sum_{l=0}^{\infty}\sum_{m=0}^{\infty}\sum_{n=0}^{\infty}\frac{1}{(2l+1)(2m+1)(2n+1)}\\ &\times\cos\frac{(2m+1)\pi x}{2a}\cos\frac{(2m+1)\pi y}{2b}\\ &\times\cos\frac{(2n+1)\pi z}{2c}\,e^{-\alpha_{l,m,n}t}, \end{aligned} \tag{6}$$

where

$$\alpha_{l,m,n}=\frac{\pi^2}{4}\left[\frac{D_0(2l+1)^2}{a^2}+\frac{D_0(2m+1)^2}{b^2}+\frac{D_e(2n+1)^2}{c^2}\right].$$

The average proton concentration, $\overline{C}(x,t)$, of the shaded slab is

$$\begin{aligned} \overline{C}(x,t)&=\frac{\int_{-c}^{c}\int_{-b}^{b}\int_{x-d/2}^{x+d/2}C(x,y,z,t)\,dx\,dy\,dz}{d2b2c}\\ &=C_s-\frac{1024a(C_s-C_0)}{d\pi^6}\\ &\quad\times\sum_{l=0}^{\infty}\sum_{m=0}^{\infty}\sum_{n=0}^{\infty}\frac{1}{(2l+1)^2(2m+1)^2(2n+1)^2}\\ &\quad\times\sin\frac{(2l+1)\pi d}{4a}\cos\frac{(2l+1)\pi x}{2a}\,e^{-\alpha_{l,m,n}t}. \end{aligned} \tag{7}$$

For large value of the time t, the series in Eq. (7) converges very rapidly and $\overline{C}(x,t)$ is very nearly given by its first term, $l=m=n=0$. That is

$$\overline{C}(x,t)\approx C_s-\frac{1024a(C_s-C_0)}{d\pi^6}\sin\left(\frac{\pi d}{4a}\right)\cos\left(\frac{\pi x}{2a}\right)e^{-\alpha_{0,0,0}t}, \tag{8}$$

where

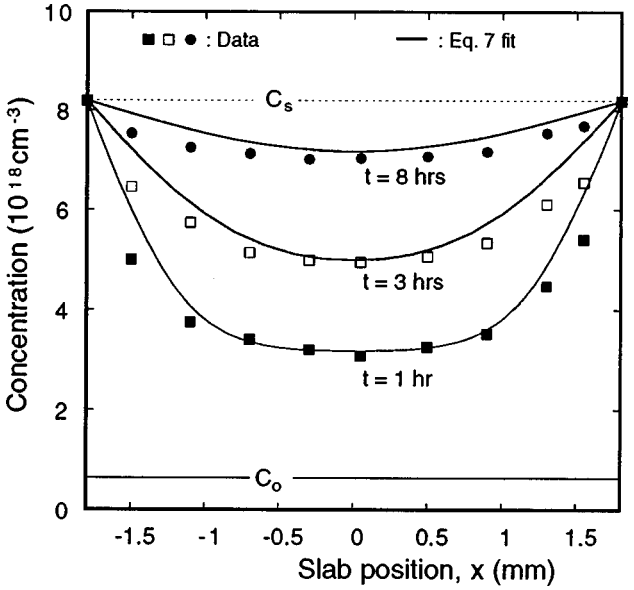

FIG. 7. Dependence of the proton concentration on the slab position x and heat treatment time t. Heat treatment temperature is 750 °C.

$$\alpha_{0,0,0}=\frac{\pi^2}{4}\left[\frac{D_0}{a^2}+\frac{D_0}{b^2}+\frac{D_e}{c^2}\right].$$

Thus, if the logarithm of $C_s-\overline{C}(x,t)$ at any point x is plotted against time t, this curve will ultimately become a straight line of slope, $-\alpha_{0,0,0}$:

$$\ln\{C_s-\overline{C}(x,t)\}\approx\ln\left[\frac{1024a(C_s-C_0)}{d\pi^6}\sin\left(\frac{\pi d}{4a}\right)\cos\left(\frac{\pi x}{2a}\right)\right]-\alpha_{0,0,0}t. \quad (9)$$

In Fig. 8, $\ln\{C_s-\overline{C}(x,t)\}$ at $x=0$ is plotted as a function of time t. After $t=2$ h, this curve showed an almost linear relation with slope of $-\alpha_{0,0,0}\approx-0.219\ \mathrm{h}^{-1}$. Since the crystal has tetragonal symmetry, the diffusivity along the c axis, D_e, may be different from D_0, the diffusivity along the a or b axis. However, the third term in $\alpha_{0,0,0}$, D_e/c^2, will have a relatively lower influence on the measured slope due to the large c value ($=2.9$ mm) compared with a ($=1.8$ mm) and b ($=1.55$ mm) unless D_e is much higher than D_0. If we assume $D_0\approx D_e$ as an approximation,

$$\frac{\pi^2}{4}\left[\frac{D_0}{a^2}+\frac{D_0}{b^2}+\frac{D_e}{c^2}\right]\approx\frac{\pi^2 D_0}{4}\left[\frac{1}{a^2}+\frac{1}{b^2}+\frac{1}{c^2}\right]\approx 0.219,$$

$$D_0\approx 0.105\times10^{-2}\ \mathrm{cm}^2/h = 0.292\times10^{-6}\ \mathrm{cm}^2/\mathrm{s}\quad \text{at } 750\ ^\circ\mathrm{C}. \quad (10)$$

This measured proton diffusivity is comparable to those reported for TiO_2 ($D_0\approx0.190\times10^{-6}$ cm^2/s) (Ref. 23) and $LiNbO_3$ ($D_0=0.193\sim2.507\times10^{-6}$ cm^2/s) (Ref. 21) at the same temperature. As previously mentioned, the proton concentration was calculated using the a_{OH} value for $LiNbO_3$ ($\sim9.125\times10^{-18}$ cm). $Pb_{0.5}Ba_{0.5}Nb_2O_6$ may have a different a_{OH} value and therefore the resulting proton concentrations may be different from those given here. However, the slope $-\alpha_{0,0,0}$ and the resulting diffusivity D_0 are not affected by the absolute values of proton concentrations but only by the ratios of proton concentrations, as is manifest in Eq. (9). The concentrations, $\overline{C}(x,t)$, obtained by substituting $D_0\approx D_e\approx0.105\times10^{-2}$ cm^2/h into Eq. (7) were given in Fig. 7 as solid lines and compared with the experimental data. The experimentally measured concentrations were in reasonably good agreement with Eq. (7) except near the edges of the crystal. The difference observed near the edges seems to be due to the out diffusion of protons during the heating and cooling processes when the flow of water vapor was shut off.

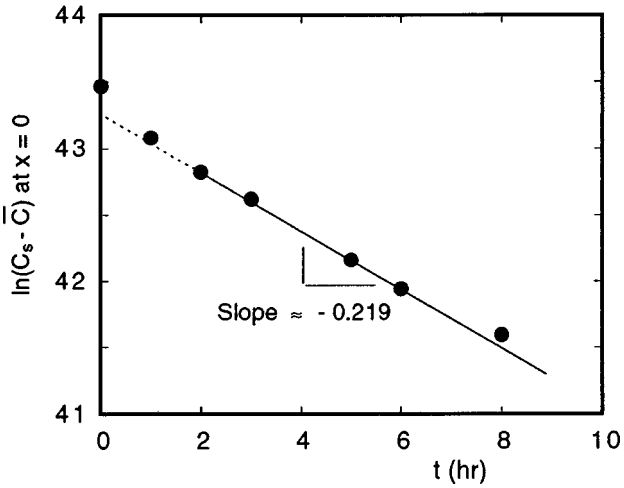

FIG. 8. $\ln\{C_s-\overline{C}(x,t)\}$ at $x=0$ as a function of time t. After $t=2$ h, this curve became linear with a slope of $-0.219\ \mathrm{h}^{-1}$.

Early investigations[9–11,24] showed that the O-H bonds in TiO_2 and $LiNbO_3$ are polarized perpendicular to the c axis. In TiO_2, the polarization of the O-H bonds perpendicular to the c axis is strikingly reflected in the diffusivities.[23,24] The diffusivity of protons along the c axis is higher than that perpendicular to the c axis, even though the O-H bonds vibrate perpendicular to the c axis. It was suggested that the large open channels parallel to the c axis in the TiO_2 structure account for the faster diffusion along the c axis.[23] Bates, Wang, and Perkins[24] proposed that the diffusion parallel to the c axis proceeds by a proton jump from one O^{-2} ion to another along the channel, and the diffusion perpendicular to the c axis proceeds by a rotation of the O-H bond to move H^+ from one channel to an adjacent channel, followed by a proton jump to another O^{-2} ion in the same channel. In $LiNbO_3$, however, the diffusivity was found to be isotropic within the experimental error.[25] Unlike TiO_2 and $LiNbO_3$, PBN has O-H bonds polarized parallel to, as well as perpendicular to, the c axis. In this study, we considered the diffusion of protons with their O-H bonds perpendicular to the c axis only because of the greater proportion of O-H bonds perpendicular than parallel to the c axis and the limited number of available crystals. The diffusion behavior of protons whose O-H bonds are polarized parallel to the c axis requires further work.

V. THERMAL DECAY OF HOLOGRAMS AND PROTON ACTIVATION ENERGY

Due to its high Curie temperature (>300 °C) and high proton concentration, PBN is a promising photorefractive

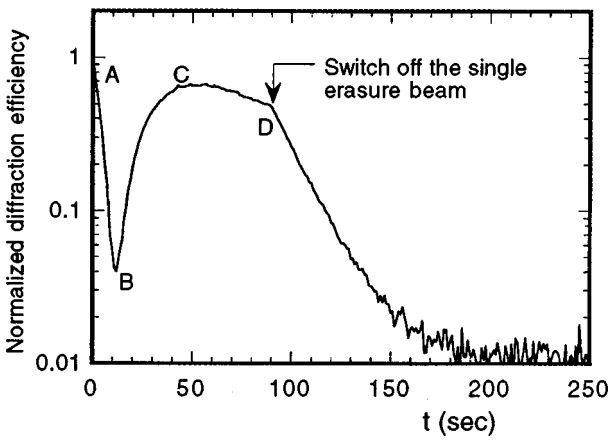

FIG. 9. Time dependence of the diffraction efficiency measured by a weak He-Ne probe beam during readout at 100 °C. Grating was written for about 2 min using two Ar^+ recording beams and then one of them was switched off at $t=0$ in order to erase the electronic grating. The single erasure beam was also turned off at D in order to reduce the beam coupling and other photoinduced effects.

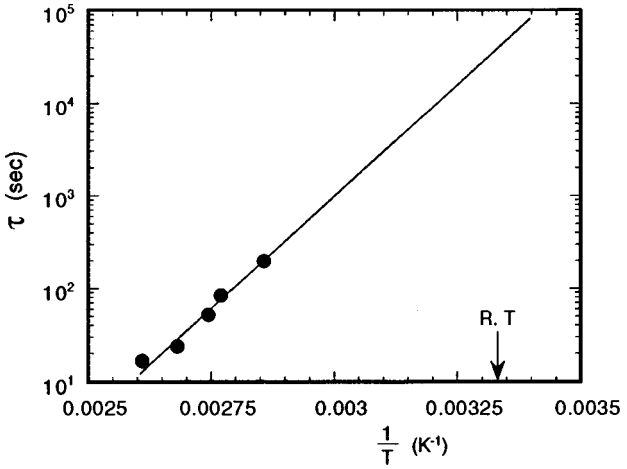

FIG. 10. $1/e$ thermal decay time of ionic grating, τ, as a function of $1/T$. The slope of the fitted line gives the activation energy, $\Delta E = 0.95 \pm 0.05$ eV.

material for nonvolatile holographic storage using the method of thermal fixing. It has recently been demonstrated that holographic gratings written in PBN50 with an Ar^+ laser can be fixed by heating the crystal above 100 °C and cooling down to room temperature before revelation.[19] In the following section, a few aspects of proton activation and transients of grating decay at various temperatures are studied.

A PBN50 sample of dimensions 1.9 mm×2.5 mm ×2.3 mm was first heated up to temperatures ranging from 70 to 110 °C, then a grating was written in the crystal with two Ar^+ beams ($\lambda = 514.5$ nm) of equal average intensities around 800 mW/cm^2. The beams were extraordinarily polarized and intersected symmetrically inside the crystal with an external angle of 32° so that the grating vector was oriented along the c axis. The diffraction efficiency, defined as the ratio of the diffracted intensity to the incident intensity, was monitored using a Bragg-matched weak He-Ne probe beam ($\lambda = 632.8$ nm). The writing times of the holograms were typically 2–3 min, so that positive ions could migrate to compensate the electronic gratings. During readout at the same elevated temperature, only one Ar^+ beam illuminated the crystal in order to erase the electronic grating and reveal the ionic grating. A typical erasure curve at elevated temperature ($T = 100$ °C) is shown in Fig. 9. At the beginning of the readout, i.e., when one of the Ar^+ beams was turned off at $t=0$, the diffraction efficiency from the total grating, consisting of both electronic and ionic components, was nonzero, indicating that the ionic compensation process was not complete, and that the total grating consisted of a larger electronic component and a smaller ionic component. During the initial phase of the readout (AB in Fig. 9), the single Ar^+ beam uniformly photoexcited trapped electrons and started erasing the electronic grating. Since the erasure of the electronic grating was fast compared with the thermal decay of the ionic grating, the diffraction efficiency of the total grating decreased until point B in Fig. 9 where the magnitude of the electronic grating was nearly the same as that of the ionic grating. The subsequent rise (BC in Fig. 9) in the diffraction efficiency indicates the revelation of the ionic grating with the continuing erasure of the electronic grating. This ionic grating is insensitive to light erasure, but can thermally decay at high temperatures. After the diffraction efficiency of the revealed grating reached a maximum (C), where the total grating consisted of mainly the ionic grating, it began to decrease due to thermal decay. It was observed that the relative maximum of the diffraction efficiency from the revealed ionic grating was larger at the higher temperature mainly due to the enhanced ion activation at higher temperature. The single Ar^+ beam was then turned off at some point (D) after this maximum in order to reduce the beam coupling and other photoinduced effects, such as charge screening effect, in the presence of the Ar^+ beam. As seen in Fig. 9, them semilogarithmic plot of the diffraction efficiency after the Ar^+ beam was turned off consists of a single exponential, indicating that there is only one ionic species participating in the ionic grating decay.

The $1/e$ decay times τ of the ionic gratings at elevated temperatures were measured with a Bragg-matched weak He-Ne probe beam in order to determine the activation energy of the ions. As shown in Fig. 10, the semilogarithmic plot of τ versus the reciprocal of temperature $1/T$ follows the Arrhenius law:

$$\tau(T) = \tau_0 \exp(\Delta E/kT), \tag{11}$$

where ΔE is the activation energy of ions. By fitting the data with Eq. (11), the thermal activation energy of ions was determined to be 0.95 ± 0.05 eV. By extrapolating the fitted line to room temperature, the ionic grating lifetime at room temperature was estimated to be 10 h in this PBN50 crystal containing $\sim 10^{19}$ cm^{-3} protons.

The measured activation energy in PBN50 is close to the proton activation energy of 1.1–1.4 eV measured in $LiNbO_3$ (Ref. 26) and 0.81–1.04 eV in $KNbO_3$.[27] Since it has been suggested in these materials that thermal fixing is made possible by protons, it is likely that protons are responsible for the formation of ionic gratings in PBN50 as well. Another indication that protons are the species responsible for the

ionic grating formation is that the diffraction efficiency of the thermally fixed grating increased with increasing proton concentration in the crystal.[20]

VI. SUMMARY

We have grown large $Pb_{1-x}Ba_xNb_2O_6$ single crystals by the vertical Bridgman method in sealed Pt crucibles in the composition range of $0.5<1-x<0.6$ with negligible PbO loss. As-grown crystals showed a strong OH^- absorption bands near $\nu=3485\ cm^{-1}$, revealing the existence of protons (H^+) which account for the formation of the secondary grating at elevated temperatures and the resulting thermal fixing of holograms. It was found that all of the O-H bonds were polarized either perpendicular or parallel to the *c* axis, with a greater density of O-H bonds perpendicular to the *c* axis. The proton concentration increased with high-temperature heat treatment in a humid atmosphere and decreased in an ambient or oxygen atmosphere. The diffusivity of protons perpendicular to the *c* axis was measured in $Pb_{0.5}Ba_{0.5}Nb_2O_6$ by proton in-diffusion experiments and was found to be $D_0=0.219\times10^{-6}\ cm^2/s$ at 750 °C, which was comparable to those in TiO_2 ($D_0=0.190\times10^{-6}\ cm^2/s$) and $LiNbO_3$ ($D_0=0.193\sim2.507\times10^{-6}\ cm^2/s$) at the same temperature. The holographic measurements showed that the electronic gratings were compensated at elevated temperatures (70–110 °C) by the ionic gratings which involved the activation and migration of protons (H^+). The proton activation energy measured in $Pb_{0.5}Ba_{0.5}Nb_2O_6$ by the thermal decay of ionic gratings was $\Delta E=0.95\pm0.05$ eV, which was close to the proton activation energies of 1.1–1.4 eV and 0.81–1.04 eV reported for $LiNbO_3$ and $KNbO_3$, respectively.

ACKNOWLEDGMENTS

This research was funded by the Defense Advanced Research Project Agency (DARPA) through the Photorefractive Information Storage Materials (PRISM) Program (Contract No. MDA 972–94–2–0008). Facilities support was provided by the NSF/MRSEC Program through the Center for Materials Research at Stanford University and by DARPA through the Center for Nonlinear Optical Materials at Stanford University. The authors wish to thank Baegin Sung in Applied Physics Department, Stanford University for his help with the high-temperature absorption measurements.

[1] J. J. Amodei and D. L. Staebler, Appl. Phys. Lett. **18**, 540 (1971).
[2] J. J. Amodei, W. Phillips, and D. L. Staebler, Appl. Opt. **11**, 390 (1972).
[3] H. Vormann, G. Weber, S. Kapphan, and E. Krätzig, Solid State Commun. **40**, 543 (1981).
[4] J. L. Brebner, S. Jandl, and Y. Lépine, Phys. Rev. B **23**, 3816 (1981).
[5] D. Houde, Y. Lépine, C. Pépin, S. Jandl, and J. L. Brebner, Phys. Rev. B **35**, 4948 (1987).
[6] I. Laulicht and L. Benguigui, Solid State Commun. **32**, 771 (1979).
[7] S. Kapphan and G. Weber, Ferroelectrics **37**, 673 (1981).
[8] O. W. Johnson, J. DeFord, and J. W. Shaner, J. Appl. Phys. **44**, 3008 (1973).
[9] W. Bollman and H. J. Stöhr, Phys. Status Solidi A **39**, 477 (1977).
[10] J. R. Herrington, B. Discher, A. Rauber, and J. Schneider, Solid State Commun. **12**, 351 (1973).
[11] L. Kovàcs, V. Szalay, and R. Capelletti, Solid State Commun. **52**, 1029 (1984).
[12] S. Hunsche, A. Gröne, G. Greten, S. Kapphan, R. Pankrath, and J. Seglins, Phys. Status Solidi A **148**, 629 (1995).
[13] R. R. Neurgaonkar, W. K. Cory, J. R. Oliver, M. D. Ewbank, and W. F. Hall, Opt. Eng. (Bellingham) **26**, 392 (1987).
[14] M. H. Francombe, Acta Crystallogr. **13**, 131 (1960).
[15] G. A. Smolensky, V. A. Isupov, and A. I. Agranovskaya, Sov. Phys. Solid State 1, 400 (1959).
[16] T. R. Shrout and L. E. Cross, Ferroelectr. Lett. **44**, 325 (1983).
[17] J. R. Oliver, R. R. Neurgaonkar, and L. E. Cross, J. Am. Ceram. Soc. **72**, 202 (1989).
[18] M. Lee, H. Lee, R. K. Route, and R. S. Feigelson, J. Appl. Phys. **81**, 917 (1997).
[19] A. Y. Liu, M. C. Bashaw, L. Hesselink, M. Lee, and R. S. Feigelson, Opt. Lett. **22**, 187 (1997).
[20] M. Lee, R. S. Feigelson, A. Y. Liu, and L. Hesselink (unpublished).
[21] S. Klauer, M. Wöhlecke, and S. Kapphan, Phys. Rev. B **45**, 2786 (1992).
[22] H. S. Carslaw and J. C. Jaeger, *Conduction of Heat in Solids*, 2nd ed. (Clarendon, Oxford, 1959), p. 185.
[23] O. W. Johnson, S.-H. Paek, and J. W. DeFord, J. Appl. Phys. **46**, 1026 (1975).
[24] J. B. Bates, J. C. Wang, and R. A. Perkins, Phys. Rev. B **19**, 4130 (1979).
[25] R. Gonzalez, Y. Chen, K. L. Tsang, and G. P. Summers, Appl. Phys. Lett. **41**, 739 (1982).
[26] A. Yariv, S. S. Orlov, and G. A. Rakuljic, J. Opt. Soc. Am. B **13**, 2513 (1996).
[27] G. Montemezzani and P. Günter, J. Opt. Soc. Am. B **7**, 2323 (1990).